NANO LETTERS

2008
Vol. 8, No. 9
2975-2981

Nanofabricated Concentric Ring Structures by Templated Self-Assembly of a Diblock Copolymer

Yeon Sik Jung, Wonjoon Jung, and C. A. Ross*

Department of Materials Science and Engineering, Massachusetts Institute of Technology, Cambridge, Massachusetts 02139

Received July 9, 2008; Revised Manuscript Received July 21, 2008

ABSTRACT

The formation of well-controlled circular patterns on the nanoscale is important for the fabrication of a range of devices such as sensors, memories, lasers, transistors, and quantum devices. Concentric, smooth ring patterns with tunable dimensions have been formed from a cylinder-forming poly(styrene-*b*-dimethylsiloxane) (PS-PDMS) diblock copolymer under confinement in shallow circular trenches. The high etch selectivity between PS and PDMS facilitates pattern transfer, illustrated by the fabrication of arrays of ferromagnetic cobalt rings with a density of 1.1 $\times$ 10^9/cm^2. The effects of confinement diameter and commensurability on the diameter and period of the concentric rings are analyzed using a free energy model that includes interfacial, strain, and bending energies. This work provides a simple process for the fabrication of nanoscale circular patterns with very narrow line width using a much coarser-scale template, and may facilitate the miniaturization of a variety of microelectronic devices.

Self-organization of macromolecular materials can provide an alternative pathway to conventional lithography for the fabrication of devices on the nanometer scale. In particular, the self-assembly of the microdomains of diblock copolymers within lithographically defined templates to create patterns with long-range order has attracted considerable attention, because of the scalability and cost-effectiveness of the process.[1,2] Devices such as field effect transistors, capacitors, flash memory cells, high density magnetic storage media, photovoltaic devices, and photonic crystals made using block copolymer patterning have been proposed or demonstrated.[3−6]

In developing self-assembly methods for device fabrication, it is important to be able to create a range of pattern geometries. One important geometry is that consisting of single or concentric rings. Several devices based on ring shaped features have been designed, including sensors,[7,8] magnetic memories,[9−11] transistors,[12] optical memories,[13] ring resonator lasers,[14] and structures used to investigate quantum interference phenomena such as the Aharonov-Bohm effect[15] or persistent currents.[16,17] As an example, three-dimensionally confined semiconductor quantum rings (or coupled concentric double quantum rings) that behave as artificial atoms have discrete energy levels that can be engineered for performing quantum computations or realizing advanced electronic or optoelectronic devices.[18,19] Self-assembly of thin films of diblock copolymers typically yields patterns consisting of parallel lines or close-packed arrays of dots or holes, and the formation of two-dimensional (2D) ring-shaped patterns suitable for device fabrication is less well explored. A self-assembly based method for creating ring patterns of controlled geometry may enable the scaling of ring-shape devices, with consequent improvements in speed or power consumption.

In this communication, we report on the templating of concentric ring patterns from cylindrical-morphology poly(styrene-*b*-dimethylsiloxane) (PS-PDMS) using topographical templates and show how these patterns can be incorporated into a device fabrication process by forming and characterizing a high-density (1.1 $\times$ 10^9/cm^2) array of ferromagnetic cobalt rings. In particular, we analyze the effects of commensurability between the diameter of the template and the period of the unconfined block copolymer. Our fabrication technique is tolerant to a wide range of processing conditions due to the robustness of the oxidized PDMS patterns and is applicable to diverse types of materials and deposition techniques.

Previous work has demonstrated both topographical[20,21] and chemical templating[22,23] as a method to improve the long-range order of self-assembled block copolymer microdomains. Although large scale 2D concentric ring patterns have been made by confinement of cylindrical or lamellar morphology block copolymers,[24−26] there has been no work reported on small diameter circular patterns where com-

* Corresponding author. E-mail: caross@mit.edu. Phone: 617-258-0223. Fax: 617-252-1020.

10.1021/nl802011w CCC: $40.75
Published on Web 08/08/2008

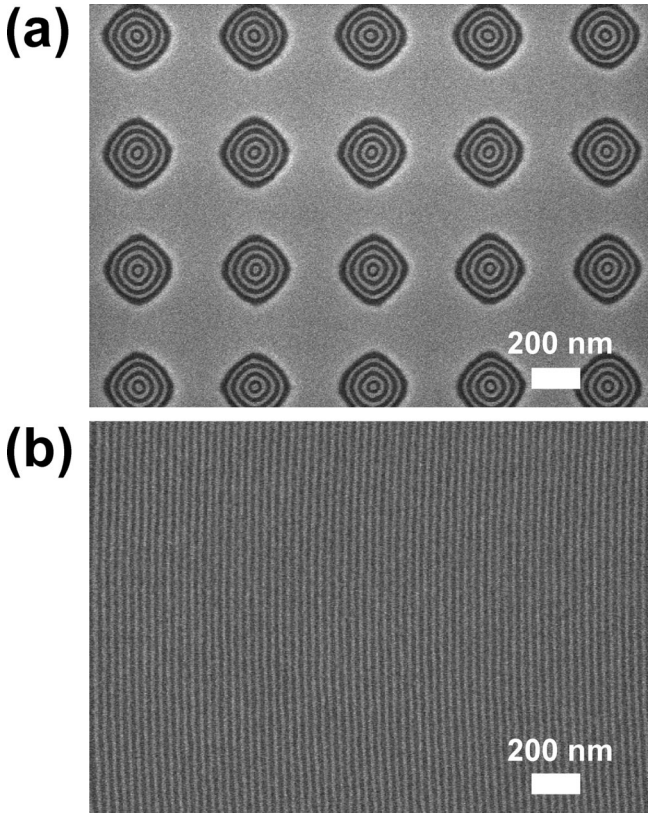

Figure 1. Morphology of the self-assembled PS-PDMS block copolymer after exposure to a CF_4 plasma (5 s) followed by an O_2 plasma (30 s). (a) Scanning electron micrograph of concentric PDMS ring patterns (light contrast) in an array of 250 nm diameter circular pits, and (b) a monolayer of well-aligned in-plane PDMS cylinders formed on a smooth substrate. Scale bars = 200 nm.

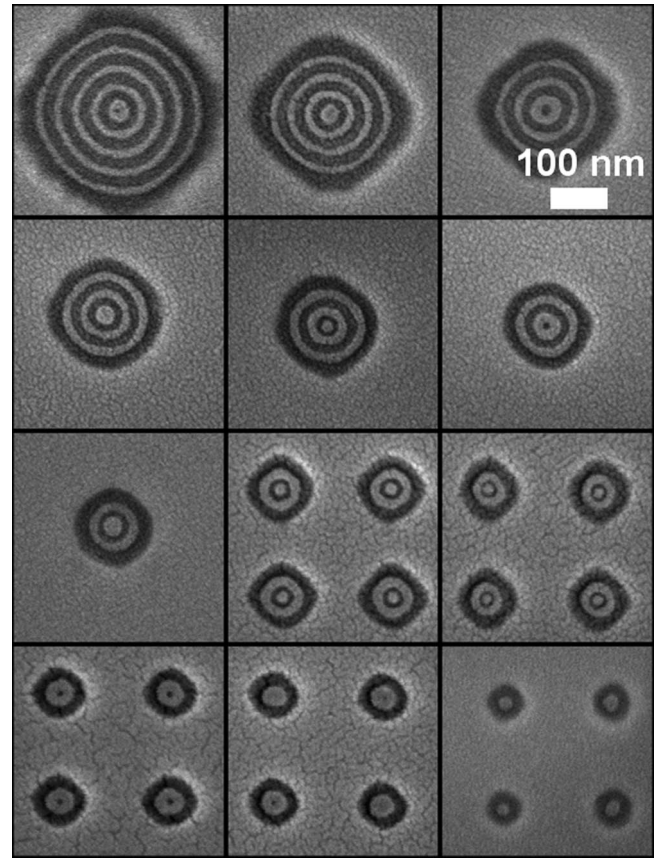

Figure 2. Concentric ring patterns in templates with various confinement diameters C. The ratio C/L_{eq} was varied from 1.7 to 10. For some diameters, the innermost feature is a PDMS sphere (light contrast) and for others a smaller PS sphere (dark) is formed. The scale bar represents 100 nm.

mensurability effects are critical. In contrast, considerable attention has been paid to understanding the three-dimensional (3D) confinement of block copolymers within cylindrical pores, both computationally[27−29] and experimentally.[30−33] However, these 3D morphologies cannot easily be incorporated into a 2D planar process for device fabrication. Nanoring arrays have been prepared using polymeric templates such as nanospheres[34] or nanoporous[35] films, obtaining, for example, 13 nm diameter rings using angled evaporation of metal into cylindrical pores.[35] However, these methods typically yield rings with 3D tapered cross sections and cannot produce concentric patterns.

We choose a PS-PDMS diblock copolymer for block copolymer lithography because of the high etch selectivity between the two blocks, the robustness of the PDMS patterns for pattern transfer, and the large correlation length and low edge roughness of the patterns.[36] The PS-PDMS (31 kg/mol for PS, 11 kg/mol for PDMS) block copolymer was spin-coated over PDMS brush-coated silica substrates prepatterned with arrays of 40 nm deep approximately circular pits of a range of diameters, then solvent-annealed and etched to reveal the arrangement of the PDMS cylinders in plane. Figure 1a shows a scanning electron micrograph of a sample of the resulting concentric rings, which were formed over large area substrates (1 cm^2) with good uniformity. The white stripes indicate the oxidized PDMS in-plane cylindrical domains after O_2 plasma reactive ion etching (RIE), about 13 nm tall, while the dark regions correspond to the volume originally occupied by the PS domains, which were removed by the RIE. The central feature in these structures is a circular PDMS domain, analogous to the central cylinder seen for lamellar block copolymers assembled in tall pores.[33] As a comparison, the same block copolymer self-assembled on a smooth substrate is presented in Figure 1b, showing the formation of parallel cylinders with large correlation length.

The circular patterns in the pits have a lower eccentricity than the templates, which resemble rounded squares, and the rings show lower edge roughness than rings made from PS-PMMA.[24] The smoothly curved structures observed here are attributed to the very large χ parameter of PS-PDMS ($\chi \sim 0.26$ at 300 K, compared with 0.06 for PS-PMMA[37,38]), which promotes the formation of geometries that minimize the interfacial area between the domains. Based on the relative χ parameters, PS-PDMS is expected to have an interfacial width of 0.95 nm, compared with 3 nm for PS-PMMA.[1] A root-mean-square roughness of 3.2 ± 0.2 nm was measured for etched PDMS patterns. In bulk, the PDMS cylinders are generally straight, and their bending into circular shapes of small radius incurs an additional energy term, which will be analyzed later. In our study, both the trench surfaces, with their grafted PDMS brush, and the air interface, due to differences in surface tension, all strongly

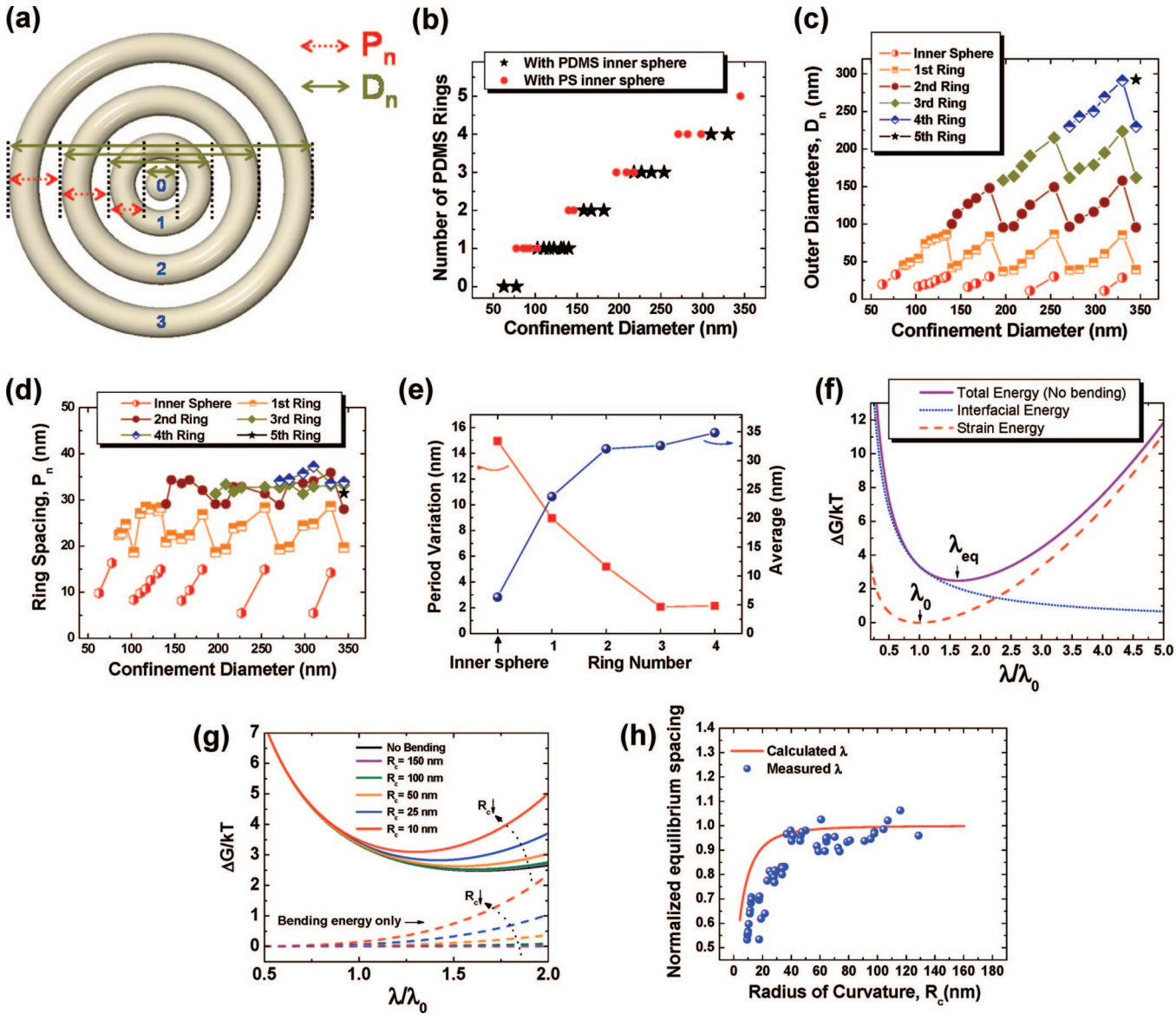

Figure 3. Manipulation of ring geometry by the design of the template, and energy analysis of concentric ring pattern formation. (a) The definition of the period P_n and outer diameter D_n of the concentric ring patterns. Here, $P_n = [D_n - D_{n-1}]/2$ or for the inner spheres, $P_0 = D_0/2$. (b) The number of concentric rings in a template as a function of its diameter, C. Stars indicate patterns with a central PDMS sphere while solid circles indicate patterns with a central PS sphere. (c) The outer diameter D_n of each PDMS ring and (d) the spacing P_n of each ring as a function of confinement diameter C. For the inner sphere, the radius is plotted. P_n and D_n show periodic fluctuations with C. The error bars in (c) are smaller than the size of the symbols. (e) The amplitude of variation ($P_{max}(n) - P_{min}(n)$) and the average P_n for each circular ring. (f) Free energy curves excluding the bending energy term. (g) Bending energy and total energy as a function of the radius of curvature (R_c). (h) Calculated equilibrium spacing λ_{eq} normalized by its value at large R_c, and measured ring spacing normalized by L_{eq}, as a function of R_c.

attract the minority PDMS block, which has a significantly lower surface tension ($\gamma = 19.9$ mN/m) than PS ($\gamma = 40.7$ mN/m).[39] The concentric PDMS ring structures in their PS matrix are therefore sandwiched between thin surface and interface PDMS brush layers.

Figure 2 illustrates how the ring patterns vary with confinement diameter C. The equilibrium period (L_{eq}) of in-plane cylinders on a smooth substrate is 34.2 nm for this polymer.[36] The ratio C/L_{eq} was varied from 1.7 to 10. For some diameters, the innermost feature is a PDMS sphere while for others a smaller PS sphere is formed. For the smallest trenches ($C < 77$ nm, $C/L_{eq} < 2.2$), only a PDMS sphere is observed. This may be compared with simulation results[29] for the self-assembly of a block copolymer in a tall, narrow cylindrical pore, in which the minority block forms a central axial feature for $2.1 < C/L_{eq} < 2.7$.

Figure 3a illustrates the definition of the period P_n and outer diameter D_n of the concentric ring patterns, where $P_n = [D_n - D_{n-1}]/2$ and D_n is the outer diameter of ring n. Figure 3b shows the number of rings formed as a function of confinement diameter C. Solid symbols and stars indicate the structures with a PS domain and a PDMS domain in the center, respectively. There is an overlap between the ranges of confinement diameter that generate a given pattern; for example, a pit of diameter 140 nm may contain either two PDMS rings with a PS inner feature or one PDMS ring plus

a center PDMS sphere, while a pit of diameter 218 nm may contain three PDMS rings with either a PS or a PDMS inner feature. Similar degeneracy has been observed in a number of confined block copolymer systems, for example, in spheres packed into trenches[20] or lamellae packed into pores,[33] where a given confinement diameter can accommodate n or $n + 1$ domains. Figure 3c,d respectively shows the variation of D_n and P_n with C. The standard deviation of measurements of ring dimensions at a given C are in the range 0.3−3 nm. For $C = 60$ or 77 nm, only a PDMS sphere appears, for 86 nm $< C <$ 94 nm, a single PDMS ring is formed without an inner sphere (so the diameter of the inner sphere is not plotted), and for 102 nm $< C <$134 nm, the inner sphere reappears, which is replaced by a second ring at $C = 140$ nm. These periodic changes in feature size and the presence or absence of the inner sphere occur throughout the whole range of confinement diameter explored here. The appearance and disappearance of the inner sphere suggest that the inner features are formed later than the outer rings, which would be consistent with other reports that the registration of block copolymer domains occurs first at the edges of lithographic patterns.[24] Each ring therefore templates the ring inside it until the final highly frustrated feature forms at the center. Figure 3e shows the amplitude of variation ($P_{max}(n) - P_{min}(n)$) and the average of P_n over the entire range of C that was tested. The spacing of the fourth and higher rings (∼34−35 nm) is similar to that of unconfined domains, L_{eq}; but the inner elements show more variation in period, and their average period is smaller. This result differs from that reported for frustrated block copolymers in tall cylindrical pores. For example, the period of lamellar-forming polystyrene−polybutadiene in anodic alumina pores was measured to be greater than the equilibrium period.[33] Simulations of lamellae confined in pores indicate that the lamellar spacing can be smaller or larger than the unconfined period and that the spacing of an inner lamella is larger than that of an outer one.[28]

To analyze the results of Figure 3d,e, we use an Alexander-de Gennes type formalism to determine the effect of domain curvature on the period of a block copolymer, assuming that the total free energy per chain is the sum of the interfacial energy and the chain conformational energy. This approach has been widely adopted for understanding lamellar, cylindrical, and spherical microphases in the strong segregation limit.[20,40−43] The reference state, wherein the free energy is zero, is the macrophase-separated homopolymers without interfaces between the different polymer blocks, or stretching of the chains. This approach gives an expression for the overall free energy ΔG as a function of domain spacing (λ): (see Supporting Information for the derivation)

$$\Delta G(\lambda) = \frac{kT}{a^2}\sqrt{\frac{\chi_{AB}}{6}}\cdot 2Na^3\cdot\frac{1}{\lambda} + \frac{1}{2}kT\cdot\left[\frac{\lambda^2}{4Na^2} + \frac{4\sqrt{Na^2}}{\lambda} - 3\right] \quad (1)$$

where k, T, a, N, γ, and Σ denote the Boltzmann constant, the temperature, the Kuhn step size, the total number of Kuhn segments, the interfacial energy/unit area, and the contact area per chain between the two blocks, respectively.

Figure 3f plots $\Delta G/kT$ per chain as a function of λ/λ_0, where λ_0 is the domain spacing for relaxed chains, where the strain energy is zero, assuming $a = 0.59$ nm, which is estimated from a weighted mean of the Kuhn step sizes of PS and PDMS reported elsewhere,[44,45] $N = 257$, and $\chi = 0.26$,[38] corresponding to the block copolymer used here. The equilibrium spacing λ_{eq} can be determined by differentiating eq 1 with respect to λ and equating to zero. The total energy for $\lambda > \lambda_{eq}$ and $\lambda < \lambda_{eq}$ is dominated by the strain energy and interfacial energy components, respectively. λ_{eq} and λ_0 are calculated to be 31.4 and 19.3 nm, respectively. The value for λ_{eq} is in reasonable agreement with the measured unconfined period of $L_{eq} = 34.2$ nm. The results for λ_{eq} and λ_0 are consistent with reports that chains are 10−40% stretched by microphase separation, compared with the relaxed state.[46,47]

However, bending brings about a significant change in the strain state of the block copolymer chains. Curving a bilayer sheet will place the inner layer in compression and the outer layer in tension, altering the layer thicknesses. For a unit layer of a diblock copolymer, this bending strain can partly be relieved by intermixing of chains, although the relaxation is limited by the connectivity between the blocks. The bending free energy per chain at a radius of curvature R_c was derived by Wang and is slightly modified here as a function of R_c and λ, using the relation $\lambda/2$ = thickness of a diblock copolymer monolayer:[48,49]

$$\Delta G^{bend}(\lambda, R_c) = \frac{\pi^2}{512}\frac{kT}{Na^2}\lambda^4\frac{1}{R_c^2} \quad (2)$$

As depicted in Figure 3g, the bending energy and consequently, the total energy rapidly increase as R_c decreases, especially for large λ since the bending energy scales with λ^4. It should be also noted that the equilibrium spacing $\lambda_{eq}(R_c)$, which corresponds to the minimum of each free energy curve, becomes smaller as R_c decreases. The equilibrium spacing λ_{eq} can be readily obtained as a function of R_c by differentiating the total energy function with respect to λ and setting it to zero. The rapid decrease of λ_{eq} with R_c is plotted in Figure 3h, where λ_{eq} has been normalized by the equilibrium spacing for unbent domains. The measured spacings of all the rings in Figure 3d are superposed on this figure, normalized by the period of the unconfined domains (34.2 nm). R_c was taken as the radius at the midpoint of each period; that is, $R_c = (D_n - P_n)/2$. Despite the approximations of the free energy model, the two data sets share the same trend, in which λ_{eq} increases rapidly with R_c for small R_c but tends toward the unconfined period for large R_c. The R_c^{-2} dependence of bending energy can therefore account for the below-equilibrium period at smaller confinement diameters depicted in Figure 3d,e.

This approach demonstrates how templates can be designed to produce self-assembled ring-shaped features with specific dimensions. We now demonstrate pattern transfer from concentric ring structures into a functional material, in this case a ferromagnetic thin film. Nanoscale ferromagnetic rings have attracted much interest due to their complex behavior and possible applications in magnetic memory, logic

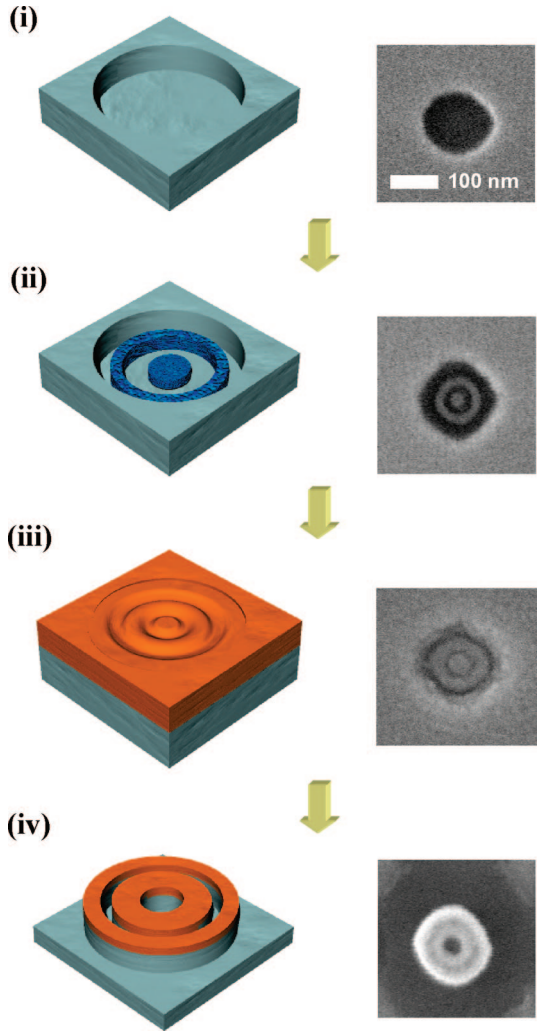

Figure 4. Cobalt double ring fabrication process. (i) Fabrication of circular trench templates using interference lithography followed by the formation of a PDMS brush using hydroxyl-terminated PDMS. (ii) Self-assembly of ring patterns in the trenches and reactive ion etching to generate oxidized PDMS ring arrays. (iii) Sputter deposition of a Co thin film (thickness = 70 nm). (iv) Dry etching with 450 W CF_4 plasma. Initially, the Co film is sputter-etched slowly by incident CF_x^+ ions, then the exposed oxidized PDMS patterns are rapidly removed through a chemical etching process. Consequently, the Co ring features form a reverse image of the original PDMS patterns.

devices, and biosensors,[7−11,50] in addition to their use for studying domain behavior and current-induced domain wall motion.[51]

Figure 4 illustrates the fabrication of concentric rings of cobalt using an image reversal process employing a CF_4 plasma. Interference lithography and etching were first employed to define a large area array of 137 nm wide and 30 nm deep circular trenches, and the PS-PDMS block copolymer was self-assembled inside the trench patterns and etched to form patterns consisting of a PDMS ring and a central PDMS sphere. A 70 nm thick Co thin film was deposited by radio frequency sputtering over the block copolymer patterns, which partly planarized the surface. A 450W CF_4 plasma was used to sputter-etch the Co film slowly at a rate of 2.3 nm/min. However, as soon as the

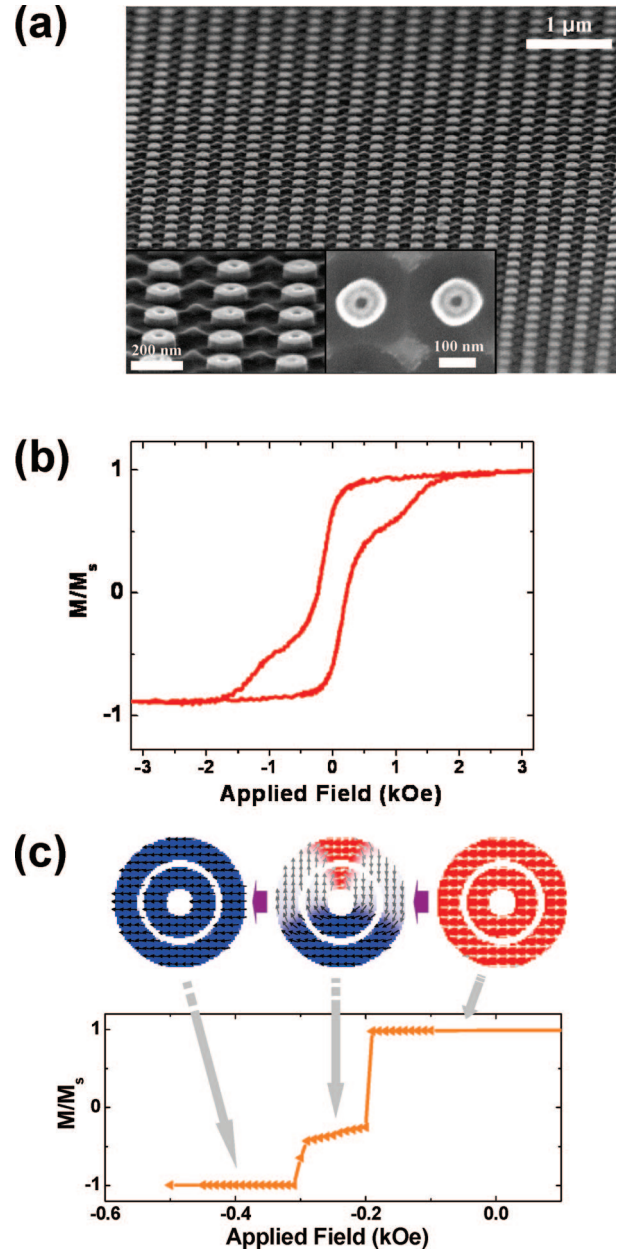

Figure 5. Pattern transfer into a ferromagnetic film. (a) SEM image of an array of Co double rings. (b) Measured and (c) simulated normalized magnetic hysteresis loops (M/M_s) of the double rings. The two rings in each structure are magnetostatically coupled, and the slanted plateau results from the formation of a distorted "vortex" state.

etch breaks through the Co film, the underlying oxidized PDMS patterns are rapidly removed by forming volatile SiF_x species. Stopping the etch at this point yielded a large array of pairs of concentric rings. The film thickness was 10 nm; the inner ring of each structure had an average outer diameter of 68 nm and a width of 16 nm, while the outer ring had an outer diameter of 133 nm and a width of 19.5 nm. The spacing between the rings was 13 nm, which is slightly smaller than the original 16 nm line width of the PDMS patterns.

Figure 5a illustrates the Co double concentric ring array. Magnetic hysteresis loops of the ring array and a half-loop derived from micromagnetic simulation are shown in Figure

5b,c, respectively. The experimental hysteresis loop is characterized by two-step switching with a slanted plateau between approximately 500 and 850 Oe. This switching behavior is reproduced qualitatively by the simulation, which shows that the two rings switch together as a result of magnetostatic interactions. As the field is reduced, the first step corresponds to a correlated onion-to-vortex transition of the rings. The nonzero moment of the correlated vortex state occurs because the vortex is off-center so that the majority of the ring material is magnetized in the direction of the reverse field. At higher reverse fields, the rings switch, again collectively, into a reverse onion state. The hysteresis loop of the double ring is not a simple superposition of that of its two component rings, each of which shows a two step reversal (onion to vortex to reverse onion state) occurring at different fields (see Supporting Information). The magnetic coupling strength between the individual rings in the multiple concentric ring configurations can be tailored by modifying the dimensions or materials of the rings, and this can control the switching field and number of stable remanent states of the structure.

This demonstration illustrates pattern transfer into a functional material from self-assembled 16 nm line width features in a large area, cost-effective, and scalable manner. Since the pattern transfer technique may be applied to other materials, the resulting well-defined circular features may be also useful in a wide range of high-performance and highly integrated devices that incorporate nanoscale rings, including transistors,[12] memories,[9−11] sensors,[7,8] quantum devices,[15−17] and lasers.[14] Scaling-down of those ring devices using templated block copolymer self-assembly to generate nanoscale ring patterns may provide a path toward higher information storage density, a faster switching time, or a lower power consumption.

Experimental Methods. The 40 nm deep circular trench patterns were fabricated using a Lloyd's Mirror interference lithography system with a 325 nm wavelength He−Cd laser. A negative resist (PS4, Tokyo Ohka Co., Ltd.) with a thickness of 200 nm was spin-coated on an oxidized Si wafer. Circular patterns on a 10 cm wafer were fabricated by exposing an interference pattern (a grating) at a dose that is lower than a full exposure condition, rotating the sample by 90°, and exposing a second grating. The dose distribution is given by the superposition of two perpendicularly aligned standing waves ($I = A\ \sin^2(\pi x/p) + A\ \sin^2(\pi y/p)$, where $2A$ is the maximum dose, p is the interference period, and x and y are the directions of the standing waves). Development results in a square array of rounded holes with their longest diameters in the x and y directions.[52] The diameter of the circular patterns was changed from 60 to 350 nm by controlling the total exposure time and the interference angle of the laser beams. Reactive ion etching with CF_4 gas was employed to transfer the circular patterns into the oxide substrate. A diblock copolymer of PS-PDMS with overall molecular weight of 45.5 kg/mol and volume fraction of PDMS $f_{DMS} = 33.5\%$ was custom-made by Polymer Source, Inc. The substrate surface was modified by hydroxy-terminated PDMS homopolymer with molecular weight 5 kg/mol, which was spin-cast and annealed at 170 °C for 15 h, then unreacted material was removed with a toluene wash. The thickness of the grafted brush layer was estimated to be 3−4 nm by ellipsometry. The PS-PDMS block copolymer films were spin-cast from a 1 wt % solution in toluene. Solvent annealing was performed at room temperature for 16 h under a controlled toluene vapor pressure.[36] Toluene vapor induces swelling of the polymer films, decreases the glass transition temperature below room temperature, and promotes rearrangement of the polymer chains. During the solvent annealing, the block copolymer flows from the mesas to the trenches,[25,36] and a careful thickness tuning was necessary to get a thickness of 35 nm PS-PDMS in the trenches without any excess polymer present on the mesa regions after solvent annealing. The annealed film was treated with a 5 s, 50 W CF_4 plasma, a 90 W O_2 plasma to remove first the PDMS surface layer, and then the PS matrix to leave oxygen-plasma-modified PDMS cylinders on the substrate.[36] The surface morphology was observed using a Zeiss/Leo Gemini 982 scanning electron microscope (SEM) operated at 5 kV. The samples were coated with a thin Au−Pd alloy film before loading in order to reduce charging effects. A Co thin film with a thickness of 70 nm was sputter-deposited (300 W, 2 mtorr) on top of the block copolymer patterns and etched with a 450 W, 10 mtorr CF_4 plasma for 25 min. Initially, the Co film is sputter-etched at 2.3 nm/min by ionized CF_x species, but after approximately 58 nm of film was removed, the buried block copolymer patterns were exposed to the plasma and then were etched about 60 times faster than the Co. Magnetic hysteresis loops were obtained from a vibrating sample magnetometer (ADE, model 1660) at room temperature. Micromagnetic modeling was carried out using the two-dimensional OOMMF software from NIST, with 2×2 nm^2 cells, 10 nm thick, and saturation magnetization $M_s = 1400$ emu/cm^3, random anisotropy $K_1 = 5.2 \times 10^6$ erg/cm^3, exchange constant $A = 1 \times 10^{-6}$ erg/cm, and damping coefficient of $\alpha = 0.5$.

Acknowledgment. The authors gratefully acknowledge Professor Edwin L. Thomas of MIT for helpful discussions, and the Semiconductor Research Corporation and a Korean Government Fellowship for financial support. The authors declare no competing financial interests.

Supporting Information Available: Free energy model for a confined block copolymer and micromagnetic simulation details. This material is available free of charge via the Internet at http://pubs.acs.org.

References

(1) Black, C. T.; Ruiz, R.; Breyta, G.; Cheng, J. Y.; Colburn, M. E.; Guarini, K. W.; Kim, H. C.; Zhang, Y. *IBM Journal of Research and Development* **2007**, *51* (5), 605–633.
(2) Darling, S. B. *Prog. Polym. Sci.* **2007**, *32* (10), 1152–1204.
(3) Black, C. T. *Appl. Phys. Lett.* **2005**, *87* (16), 163116.
(4) Deng, T.; Chen, C. T.; Honeker, C.; Thomas, E. L. *Polymer* **2003**, *44* (21), 6549–6553.
(5) Gowrishankar, V.; Miller, N.; McGehee, M. D.; Misner, M. J.; Ryu, D. Y.; Russell, T. P.; Drockenmuller, E.; Hawker, C. J. *Thin Solid Films* **2006**, *513* (1−2), 289–294.
(6) Osuji, C.; Chao, C. Y.; Bita, I.; Ober, C. K.; Thomas, E. L. *Adv. Funct. Mater.* **2002**, *12* (11−12), 753–758.

(7) Miller, M. M.; Prinz, G. A.; Cheng, S. F.; Bounnak, S. *Appl. Phys. Lett.* **2002**, *81* (12), 2211–2213.
(8) Llandro, J.; Hayward, T. J.; Morecroft, D.; Bland, J. A. C.; Castano, F. J.; Colin, I. A.; Ross, C. A. *Appl. Phys. Lett.* **2007**, *91* (20), 203904.
(9) Zhu, J. G.; Zheng, Y. F.; Prinz, G. A. *J. Appl. Phys.* **2000**, *87* (9), 6668–6673.
(10) Castano, F. J.; Morecroft, D.; Jung, W.; Ross, C. A. *Phys. Rev. Lett.* **2005**, *95* (13), 137201.
(11) Wen, Z. C.; Wei, H. X.; Han, X. F. *Appl. Phys. Lett.* **2007**, *91* (12), 122511.
(12) Watanabe, H.; Manabe, C.; Shigematsu, T.; Shimizu, M. *Appl. Phys. Lett.* **2001**, *78* (19), 2928–2930.
(13) Hill, M. T.; Dorren, H. J. S.; de Vries, T.; Leijtens, X. J. M.; den Besten, J. H.; Smalbrugge, B.; Oei, Y. S.; Binsma, H.; Khoe, G. D.; Smit, M. K. *Nature* **2004**, *432* (7014), 206–209.
(14) Pauzauskie, P. J.; Sirbuly, D. J.; Yang, P. D. *Phys. Rev. Lett.* **2006**, *96* (14), 4.
(15) Aharonov, Y. *Phys. Rev.* **1959**, *115*, 485.
(16) Levy, L. P.; Dolan, G.; Dunsmuir, J.; Bouchiat, H. *Phys. Rev. Lett.* **1990**, *64* (17), 2074–2077.
(17) Matveev, K. A.; Larkin, A. I.; Glazman, L. I. *Phys. Rev. Lett.* **2002**, *89* (9), 096802.
(18) Fuhrer, A.; Luescher, S.; Ihn, T.; Heinzel, T.; Ensslin, K.; Wegscheider, W.; Bichler, M. *Nature* **2001**, *413* (6858), 822–825.
(19) Warburton, R. J.; Schaflein, C.; Haft, D.; Bickel, F.; Lorke, A.; Karrai, K.; Garcia, J. M.; Schoenfeld, W.; Petroff, P. M. *Nature* **2000**, *405* (6789), 926–929.
(20) Cheng, J. Y.; Mayes, A. M.; Ross, C. A. *Nat. Mater.* **2004**, *3* (11), 823–828.
(21) Segalman, R. A.; Yokoyama, H.; Kramer, E. J. *Adv. Mater.* **2001**, *13* (15), 1152–1155.
(22) Rockford, L.; Mochrie, S. G. J.; Russell, T. P. *Macromolecules* **2001**, *34* (5), 1487–1492.
(23) Stoykovich, M. P.; Muller, M.; Kim, S. O.; Solak, H. H.; Edwards, E. W.; de Pablo, J. J.; Nealey, P. F. *Science* **2005**, *308* (5727), 1442–1446.
(24) Black, C. T.; Bezencenet, O. *IEEE Transactions on Nanotechnology* **2004**, *3* (3), 412–415.
(25) Sundrani, D.; Darling, S. B.; Sibener, S. J. *Langmuir* **2004**, *20* (12), 5091–5099.
(26) Wilmes, G. M.; Durkee, D. A.; Balsara, N. P.; Liddle, J. A. *Macromolecules* **2006**, *39* (7), 2435–2437.
(27) He, X. H.; Song, M.; Liang, H. J.; Pan, C. Y. *J. Chem. Phys.* **2001**, *114* (23), 10510–10513.
(28) Li, W. H.; Wickham, R. A.; Garbary, R. A. *Macromolecules* **2006**, *39* (2), 806–811.
(29) Yu, B.; Sun, P. C.; Chen, T. C.; Jin, Q. H.; Ding, D. T.; Li, B. H.; Shi, A. C. *Phys. Rev. Lett.* **2006**, *96* (13), 138306.
(30) Shin, K.; Xiang, H. Q.; Moon, S. I.; Kim, T.; McCarthy, T. J.; Russell, T. P. *Science* **2004**, *306* (5693), 76–76.
(31) Wu, Y. Y.; Cheng, G. S.; Katsov, K.; Sides, S. W.; Wang, J. F.; Tang, J.; Fredrickson, G. H.; Moskovits, M.; Stucky, G. D. *Nat. Mater.* **2004**, *3* (11), 816–822.
(32) Wu, Y. Y.; Livneh, T.; Zhang, Y. X.; Cheng, G. S.; Wang, J. F.; Tang, J.; Moskovits, M.; Stucky, G. D. *Nano Lett.* **2004**, *4* (12), 2337–2342.
(33) Xiang, H. Q.; Shin, K.; Kim, T.; Moon, S. I.; McCarthy, T. J.; Russell, T. P. *Macromolecules* **2004**, *37* (15), 5660–5664.
(34) Zhu, F. Q.; Chern, G. W.; Tchernyshyov, O.; Zhu, X. C.; Zhu, J. G.; Chien, C. L. *Phys. Rev. Lett.* **2006**, *96*, 2.
(35) Singh, D. K.; Krotkov, R. V.; Xiang, H.; Xu, T.; Russell, T. P.; Tuominen, M. *Nanotechnology* **2008**, *19* (24), 245305.
(36) Jung, Y. S.; Ross, C. A. *Nano Lett.* **2007**, *7* (7), 2046–2050.
(37) Bucholz, T. L.; Loo, Y. L. *Macromolecules* **2006**, *39* (18), 6075–6080.
(38) Nose, T. *Polymer* **1995**, *36* (11), 2243–2248.
(39) Chan, C. M., *Polymer Surface Modification and characterzation*, 1st ed.; Hanser Publishers: Munich, 1994.
(40) Alexander, S. *Journal De Physique* **1977**, *38* (8), 977–981.
(41) Degennes, P. G. *Macromolecules* **1980**, *13* (5), 1069–1075.
(42) Frischknecht, A.; Fredrickson, G. H. *Macromolecules* **1999**, *32* (20), 6831–6836.
(43) Gido, S. P.; Thomas, E. L. *Macromolecules* **1997**, *30* (13), 3739–3746.
(44) Matsuno, R.; Otsuka, H.; Takahara, A. *Soft Matter* **2006**, *2* (5), 415–421.
(45) Senden, T. J.; di Meglio, J. M.; Auroy, P. *Euro. Phys. J. B* **1998**, *3* (2), 211–216.
(46) Gido, S. P.; Schwark, D. W.; Thomas, E. L.; Goncalves, M. D. *Macromolecules* **1993**, *26* (10), 2636–2640.
(47) Helfand, E.; Wasserman, Z. R. *Macromolecules* **1980**, *13* (4), 994–998.
(48) Wang, Z. G. *J. Chem. Phys.* **1994**, *100* (3), 2298–2309.
(49) Wang, Z. G.; Safran, S. A. *J. Chem. Phys.* **1991**, *94* (1), 679–687.
(50) Castano, F. J.; Ng, B. G.; Colin, A.; Morecroft, D.; Jung, W.; Ross, C. A. *J. Phys. D: Appl. Phys.* **2008**, 41.
(51) Klaui, M.; Vaz, C. A. F.; Bland, J. A. C.; Wernsdorfer, W.; Faini, G.; Cambril, E.; Heyderman, L. J. *Appl. Phys. Lett.* **2003**, *83* (1), 105–107.
(52) Farhoud, M.; Ferrera, J.; Lochtefeld, A. J.; Murphy, T. E.; Schattenburg, M. L.; Carter, J.; Ross, C. A.; Smith, H. I. *J. Vacuum Sci. Technol. B* **1999**, *17* (6), 3182–3185.

NL802011W